



Article

A Study on the Effects of Cementless Total Knee Arthroplasty Implants' Surface Morphology via Finite Element Analysis

Peter J. Hunt ^{1,†}, Mohammad Noori ¹, Scott J. Hazelwood ², Naudereh B. Noori ^{3,*} and Wael A. Altabey ^{4,*}

¹ Department of Mechanical Engineering, California Polytechnic State University, San Luis Obispo, CA 93405, USA; mnoori52@yahoo.com (M.N.)

² Department of Biomedical Engineering, California Polytechnic State University, San Luis Obispo, CA 93405, USA

³ Department of Orthopedic Surgery, University of California-Irvine, Orange, CA 92868, USA

⁴ Department of Mechanical Engineering, Faculty of Engineering, Alexandria University, Alexandria 21544, Egypt

* Correspondence: nboori@uci.edu (N.B.N.); wael.altabey@gmail.com (W.A.A.)

† This work was part of the Master's thesis of the first author Peter J. Hunt.

Abstract: Total knee arthroplasty (TKA) is one of the most commonly performed orthopedic surgeries, with nearly one million performed in 2020 in the United States alone. Changing patient demographics, predominately indicated by increases in younger, more active, and more obese patients undergoing TKA, poses a challenge to orthopedic surgeons as these factors present a greater risk of long-term complications. Historically, cemented TKA has been the gold standard for fixation, but long-term aseptic loosening continues to be a risk for cemented implants. Cementless TKA, which relies on the surface morphology of a porous coating for biologic fixation of implant to bone, may provide improved long-term survivorship compared with cement. The quality of this bond is dependent on an interference fit and the roughness, or coefficient of friction, between the implant and the bonebone. Stress shielding is a measure of the difference in the stress experienced by implanted bone versus surrounding native bone. A finite element model (FEM) can be used to quantify and better understand stress shielding in order to better evaluate and optimize implant design. In this study, a FEM was constructed to investigate how the surface coating of cementless implants (coefficient of friction) and the location of the coating application affected the stress-shielding response in the tibia. It was determined that the stress distribution in the native tibia surrounding a cementless TKA implant was dependent on the coefficient of friction applied at the tip of the implant's stem. Materials with lower friction coefficients applied to the stem tip resulted in higher compressive stress experienced by implanted bone, and more favorable overall stress-shielding responses.



Citation: Hunt, P.J.; Noori, M.; Hazelwood, S.J.; Noori, N.B.; Altabey, W.A. A Study on the Effects of Cementless Total Knee Arthroplasty Implants' Surface Morphology via Finite Element Analysis.

BioMedInformatics **2024**, *4*, 1425–1440.
<https://doi.org/10.3390/biomedinformatics4020078>

Academic Editor: Alexandre G. De Brevern

Received: 22 January 2024

Revised: 25 April 2024

Accepted: 27 May 2024

Published: 3 June 2024



Copyright: © 2024 by the authors. Licensee MDPI, Basel, Switzerland. This article is an open access article distributed under the terms and conditions of the Creative Commons Attribution (CC BY) license (<https://creativecommons.org/licenses/by/4.0/>).

1. Introduction

Patient demographics for total knee arthroplasty (TKA) recipients are trending both younger and heavier [1,2]. It is projected that by 2030, 55% of all TKAs will be implanted in patients younger than 65 years [3]. With this change comes an increased concern for aseptic loosening of cemented implants over time due to the greater mechanical stress from weight and the need for greater implant longevity in younger, active patients.

Historically, aseptic loosening has been a leading cause of failure after TKA for both cemented and cementless implants [4]. Aseptic loosening is primarily the result of implant wear leading to debris, causing peri-implant osteolysis which leads to painful implant subsidence. Improvements in polyethylene manufacturing have decreased rates of this osteolysis [5]. However, there remains concern of loosening at the cement–bone interface, leading to subsequent late loosening and failure, particular in heavier and younger patients.

Cementless TKA was initially developed to decrease this risk via biologic fixation. [6,7] Early generations of cementless TKA had high failure rates due to insufficient and inadequate surface coating, and poor component geometry [8]. Newer designs have improved characteristics; biologic fixation is achieved by a porous or roughened surface, which promotes ingrowth and ongrowth osseointegration. If appropriate biological fixation occurs, it may decrease the likelihood of implant aseptic loosening and increase survivorship [7,9].

Stress shielding can contribute to implant wear at the cement–bone interface [10,11]. Stress shielding is a comparison of the stress distribution between two materials, and is a mechanical measure of the bone–implant relationship.

While the topic of optimal implant design has been widely discussed, there is limited literature on the optimal surface coating applied to cementless TKA implants. Most previous literature has been confined to experimental studies on the femoral TKA component. These studies established that postoperative primary fixation for cementless implants depends on the magnitude of the interference fit and the coefficient of friction [12–15]. These studies concluded that a higher coefficient of friction achieves superior primary fixation. In addition, Damm et al. found that if perfect osseointegration is achieved, the bone and implant are assumed to be rigidly bonded to each other, allowing no relative motion and reducing the relevancy of the coefficient of friction [12].

While these studies contribute to the understanding of cementless implant design, the limitations of their scope leave room for improving the optimal cementless implant surface morphology. To the author's knowledge, there are no studies that have analyzed the effects of surface morphologies in the tibia, and by proxy, analyzed how surface morphologies affect stress shielding in the tibia.

A FEM was constructed to evaluate different surface morphologies for cementless TKA implants and stress shielding experienced in the tibia. Surface morphology was varied by the coating's frictional properties and the location of its application. In the event of perfect osseointegration, the friction coefficient becomes irrelevant; therefore, this study only considered an implant prior to achieving biologic fixation. To comply with the mechanical nature of the selected variables, stress shielding was selected as the output and was determined by measurement of minimum principal stress.

2. Methods

2.1. Implant Model

SolidWorks (Dassault Systemes, San Diego, CA, USA) was used to construct a 3D model of a tibial TKA component (Figure 1), based on the geometry of DePuy Synthes' Attune® Total Knee System, an implant specifically designed for cementless fixation. The dimensions of relevant geometric features of the implant are shown in Table 1.

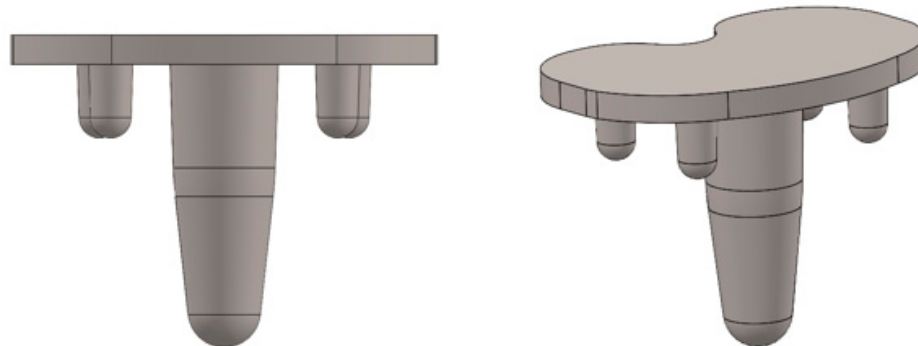


Figure 1. Implant geometry.

Table 1. Implant dimensions.

Geometric Feature	Dimension
Stem	Diameter: ~14.7 mm Length: ~40 mm
Pegs	Diameter: 6 mm Length: 10 mm
Baseplate	Thickness: 4 mm

After construction in SolidWorks, the implant part file was imported to ABAQUS (Dassault Systemes, San Diego, CA, USA), where its material was assigned as titanium. It was assumed that the implant was linear-elastic, homogeneous, and isotropic. See Table 2 for material properties.

Table 2. Material properties.

Material	Young's Modulus (GPa)	Poisson's Ratio
Titanium	110	0.3
Cortical bone	14.2	0.3
Trabecular bone	1.75	0.3

2.2. Bone Model

A CT scan of a synthetic human tibia served as the reference geometry for the tibia. This model was provided by Pacific Research Labs, in a public domain as an STL file. Pre-processing of the tibia was performed with MESHLAB (Pisa, Italy) and SolidWorks. To reduce the finite element (FE) computational effort, only the proximal tibia was modeled, and the distal portion removed, as governed by St. Venant's principal.

To model cortical and trabecular bone, SolidWorks was used to create a part file for each bone type. Cortical bone was modeled to be uniformly 3 mm thick. Both cortical and trabecular bone were modeled to be linear-elastic, homogeneous, and isotropic. The linear assumption allowed for the definition of the bone with two independent properties—Young's modulus and Poisson's ratio—which were selected based on reported values. See Table 2 for material properties.

2.3. Interactions

The interfaces between the implant, trabecular bone, and cortical bone were modeled in the FEM using interactions defined in ABAQUS. A tie constraint was assigned to the adjacent surfaces between the trabecular and cortical bone to prevent any relative motion between them.

Modeling the porous coated surfaces in a FEM would require discretization of the pores' microstructure, a computationally extensive task. Thus, to simplify the computational effort, the properties of porous coated surfaces were distilled down to their coefficient of friction and modeled in ABAQUS using the Coulomb friction definition. To input the coating's coefficient of friction, a surface-to-surface contact interaction was created between implant and bone surfaces. Similarly, the relationship between uncoated regions of the implant and bone were also governed by the coefficient of friction and modeled in ABAQUS with a surface-to-surface contact. The uncoated portions of the implant were assigned a friction coefficient of 0.15, as indicated by Damm [12].

The interference fit was not included in this study because its inclusion into the model would result in unreasonably high stresses in the bone, prohibiting a direct comparison between the coefficient of friction and stress distribution [12,16]. To preserve model integrity with respect to the desired outputs, the fit between the bone and implant was assumed to be perfect.

2.4. Applied Loads and BCs

To ensure loads were purely compressive, the knee was assumed to be fully extended. Prior work has shown that the maximum force at the tibiofemoral joint averages about 3 times body weight [17]. Therefore, a 2400 N force was set as the maximum loading condition, which corresponds to the average North American's weight of about 82 kg (180 lb) [18].

The total tibiofemoral load was applied to the medial and lateral condyles. A study by Zhao et al. concluded that there was a consistent 55% medial and 45% lateral tibiofemoral load distribution; these breakdowns were used in this study to define 1320 N and 1080 N as the medial and lateral loads, respectively [19]. The loads were incorporated into ABAQUS as uniform pressure distributions; the location and size of their contact areas were determined based on contact patterns determined by Fukubayashi and Kurosawa [20]. The distal end of the tibia was assigned a fixed constraint.

2.5. Mesh Generation

The assembly was meshed using ABAQUS's built-in free-meshing technique (Figure 2). To mesh the bone and the implant, 10-node C3D10 elements were selected due to their proficiency with complex geometry.

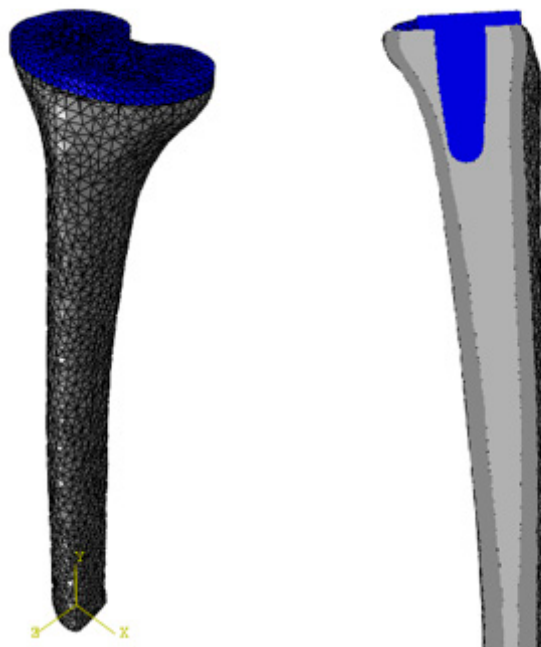


Figure 2. Meshed assembly.

Convergence studies on each of the part files indicated that an element size of around 2 mm provided suitable results. These checks were performed by observing the minimum principal stress at twelve specific locations (four on each of the parts) and comparing their change with successive models meshed with different-sized elements. Importantly, the final element sizes for all parts were similar, mitigating the risk of geometric discontinuities at the part interfaces.

2.6. Configurations

To analyze how the surface morphologies of cementless implants affected stress shielding, a total of sixteen different configurations, varying the coated-surfaces' friction coefficient and the location of its application, were constructed. Four different types of coatings were chosen based on reported values (Table 3 and Figure 3). These coatings

were applied to four different coating–location configurations, based on examination of commercially available cementless implants.

Table 3. Friction coefficients of coatings. Uncoated is shown for reference.

Description	Coefficient of Friction
Uncoated	0.15
Grit-blasted	0.5
Porocoat	0.95
DePuy Synthes experimental	1.4
High control	2

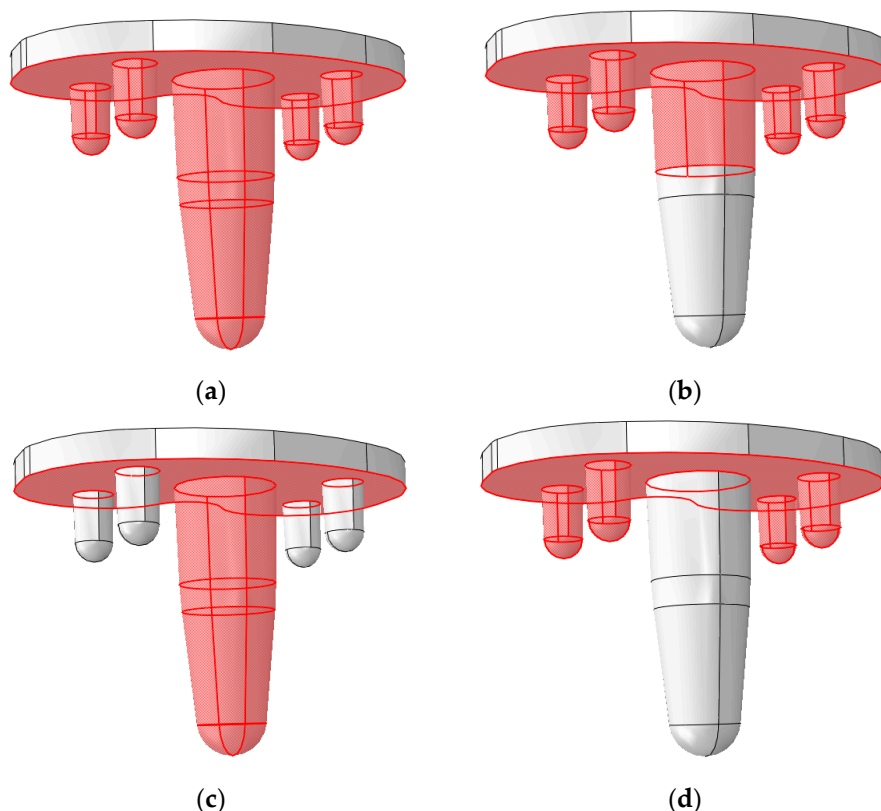


Figure 3. Configurations of coating locations. (a) Fully coated, (b) partial stem, (c) full stem, and (d) just pegs.

2.7. Post-Processing

Stress shielding in the trabecular bone was calculated with Equation (1):

$$\text{Stress Shielding} = \frac{\text{Minimum Principal Stress in Implanted Tibia}}{\text{Minimum Principal Stress in Intact Tibia}} \quad (1)$$

where stress shielding is reported as a ratio. A value of less than one is an indicator of stress shielding where the post-TKA bone experiences a decrease in stress compared with the intact tibia; smaller numbers correspond to greater stress shielding. Since the applied loads were purely compressive, the minimum principal stress was used as the stress measure in this study, as it is the most compressive of the principal stresses.

Minimum principal stresses in the implanted and intact tibia were computed as an average over a region. Regions were created in two steps. First, planes of elements were created at 10 mm axial intervals to a depth of 70 mm. Then, each of these sections was divided into four anatomical quadrants, resulting in 32 regions where stress shielding was computed (see Figure 4).

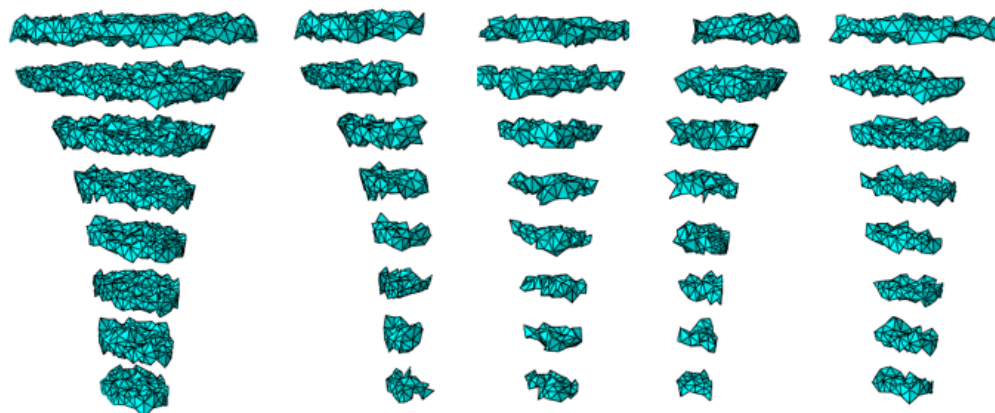


Figure 4. Elemental sets used to define the intact tibia stress. From left to right: plane of elementals prior to being divided into anatomical quadrants, medial elemental set, posterior elemental set, lateral elemental set, and anterior elemental set.

3. Results

Results were broken up into stress-shielding analysis and stress-concentration analysis. The stress-shielding results refer to the analysis of the entire bone-implant system, or 'global' results. The stress-concentration results were determined by analysis of the stress concentrations in specific regions of bone near distinguishing features of the implant (i.e., tip of stem and pegs), or 'local' results. For both results, the effects of coating location and coefficient of friction were analyzed as one variable was varied and the other remained constant.

3.1. Global Results: Optimal Coefficient of Friction

To determine the optimal coefficient of friction, the coating configurations were held constant as the friction coefficient varied. The stress-shielding results in the medial compartment for different coating configurations are seen in Figure 5; the stress-shielding values for the lateral, posterior, and anterior compartments displayed the same trends as that seen in the medial compartment. Figure 5 indicates a high level of similarity between the fully coated and just-stem configurations as well as between the partially coated and just-pegs configurations. However, the results were not identical, with variation among them in the regions in contact with, or proximity to, the implant.

Figure 5 also demonstrates that stress shielding was greatest at depths of 0 mm to 30 mm from the resectioned plane. At these depths, all configurations saw improved stress-shielding values with decreasing values of the coefficient of friction.

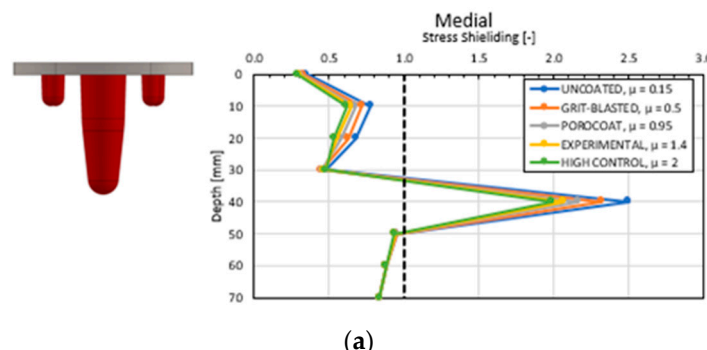


Figure 5. Cont.

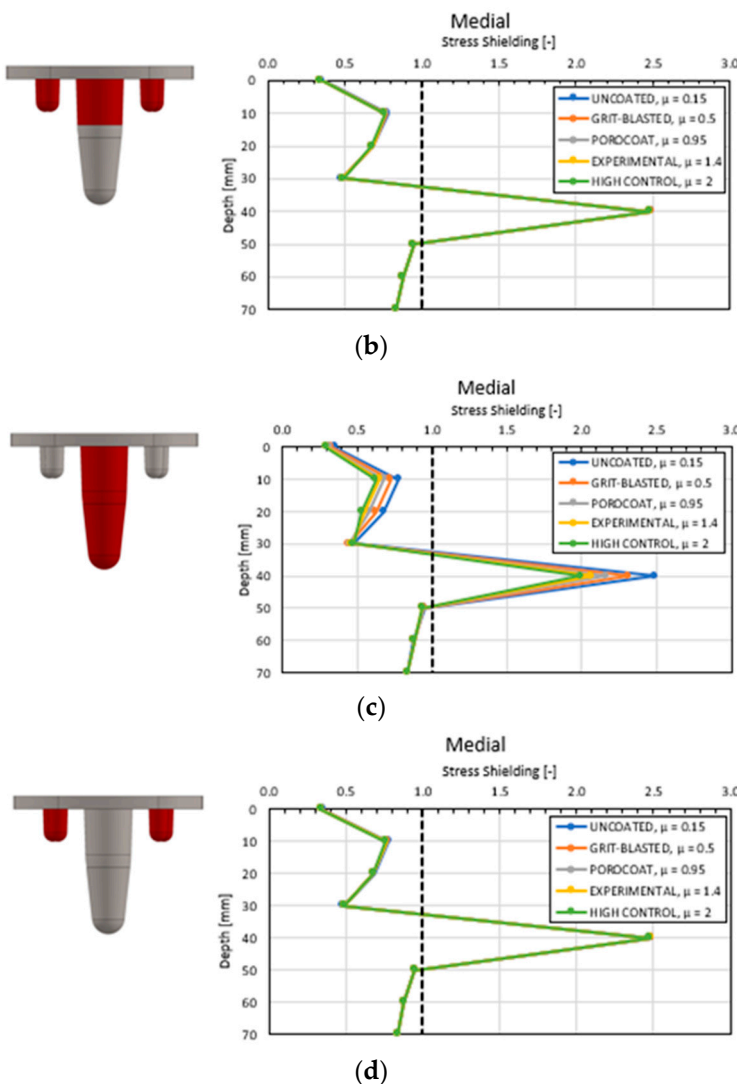


Figure 5. Stress-shielding response in the medial compartment for the (a) fully coated, (b) partially coated, (c) just-stem, and (d) just-pegs configurations. All other anatomical compartments displayed similar trends.

3.2. Global Results: Optimal Coating Location

To determine the optimal coating location, the coefficients of friction were held constant as the coating location varied. Figure 6 shows the stress shielding in the posterior compartment for different coating configurations.

The results in Figure 6 show a consistent similarity between the fully coated and just-stem configurations, and the partially coated and just-pegs configurations (note that their curves appear as one in Figure 6). The stress shielding of the fully coated and just-stem configurations increased as the coefficient of friction increased. As per Equation (1), the partially coated and just-pegs configurations exhibited superior stress-shielding performance at all friction coefficients.

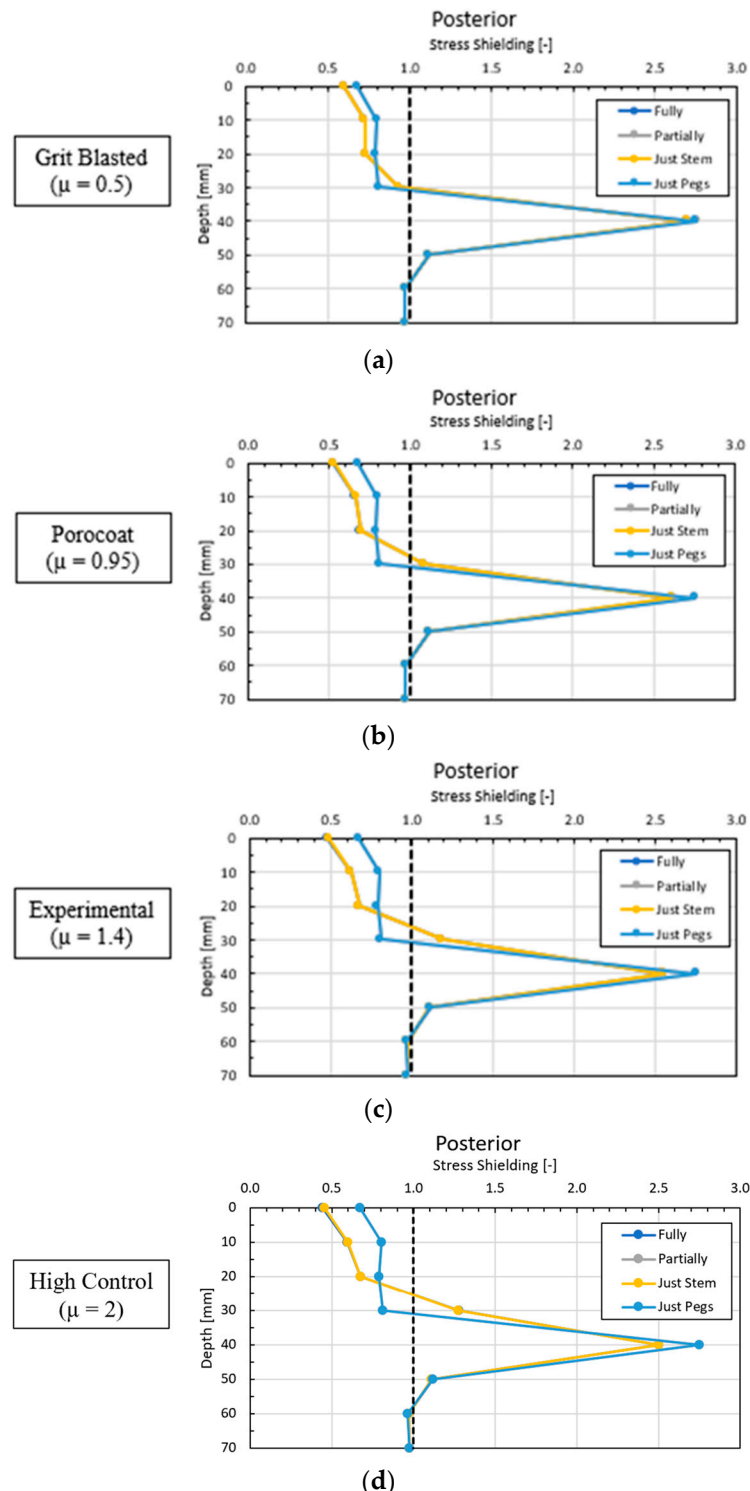


Figure 6. Stress-shielding response in the posterior compartment for implants with (a) grit-blasted, (b) Porocoat, (c) experimental, and (d) high control coatings.

3.3. Local Results: Optimal Coefficient of Friction

A comparison of the stress concentrations at the tips of the pegs and stem was conducted to determine the coefficient of friction that minimized the magnitude of the stress concentrations. Each coating location configuration was held constant as the coefficient of friction varied. Figure 7 contains the results of the stress concentrations when subjected to varying friction coefficients. Across all configurations, a smaller coefficient of friction

resulted in greater stress concentration. Again, the fully coated and just-stem configurations demonstrated similar responses, and the partially coated and just-pegs configurations were comparable in their trends.

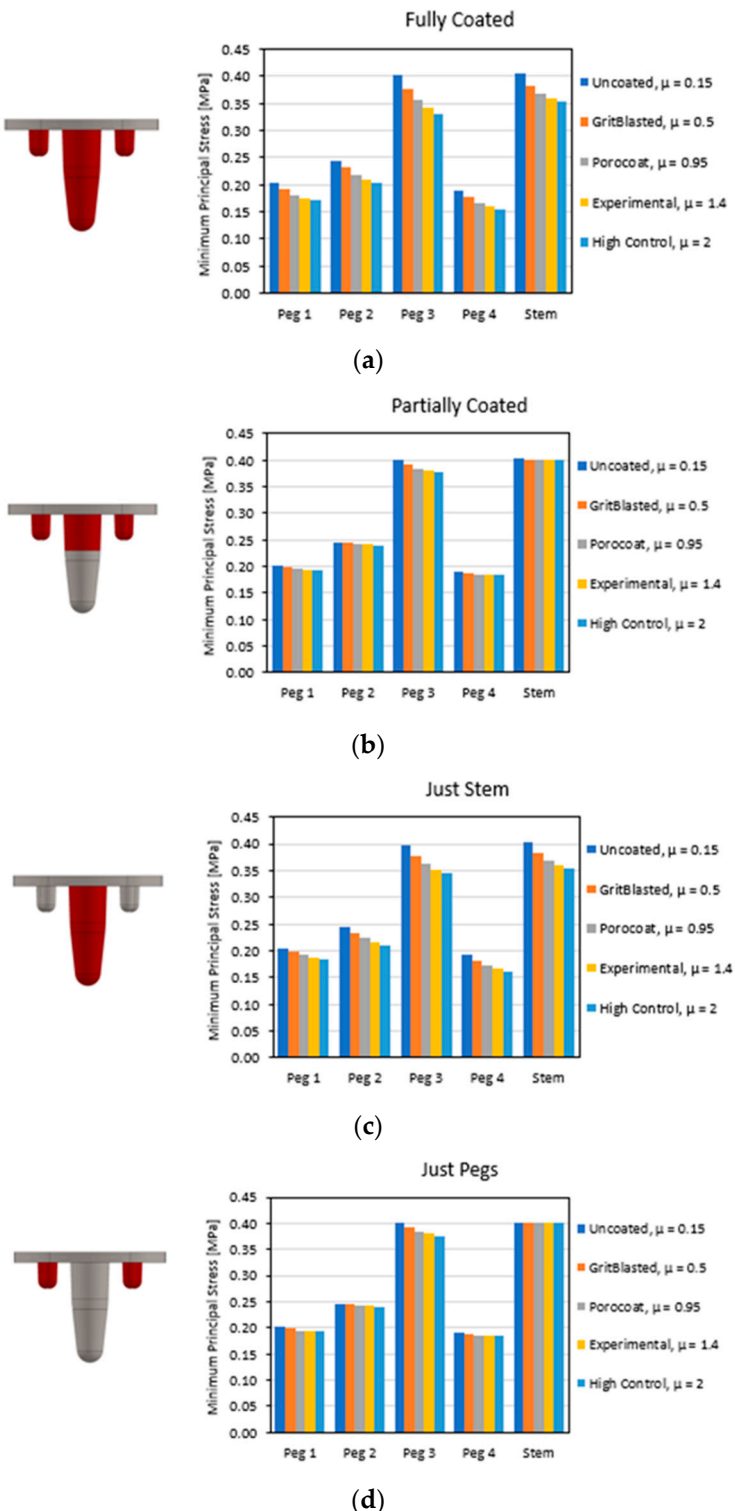


Figure 7. Stress concentrations measured for the (a) fully coated, (b) partially coated, (c) just-stem, and (d) just-pegs configurations.

3.4. Local Results: Optimal Coating Location

To determine the optimal coating location which best minimized stress concentrations, the coating locations were varied as the friction coefficient remained constant. Figure 8 depicts the stress-concentration results as the coating location was varied.

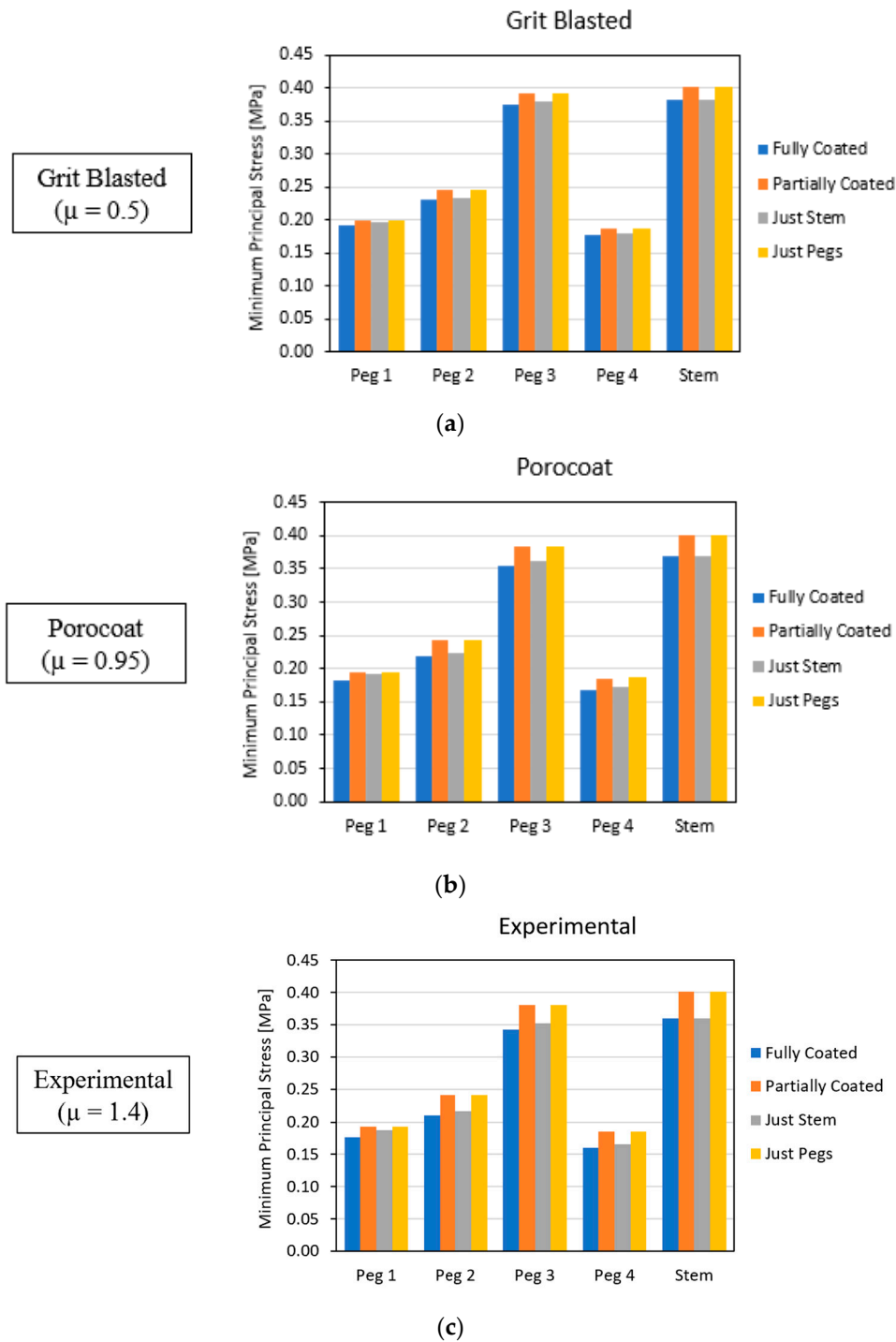


Figure 8. Cont.

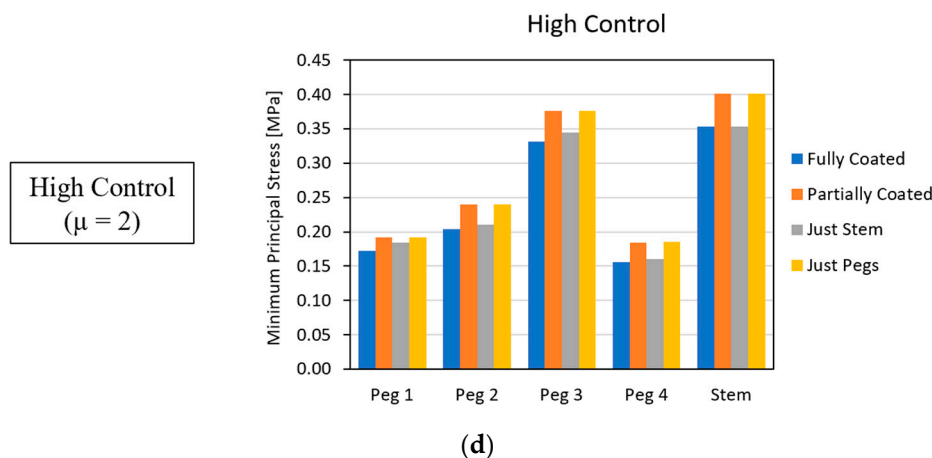


Figure 8. Stress concentrations for implants with (a) grit-blasted, (b) Porocoat, (c) experimental, and (d) high control coatings.

Across all coefficients of friction, the partially coated and just-pegs configurations exhibited larger stress-concentration magnitudes than the fully and just-stem configurations. Again, the results for the partially coated and the just-pegs configurations were very similar; likewise, the results for the fully coated and just-stem configurations showed comparable behavior.

4. Discussion

The fully coated and just-stem configurations had similar global and local trends. Likewise, the partially coated and just-pegs configurations demonstrated comparable behavior. In terms of the optimal coefficient of friction, the global results supported the conclusion that a smaller value will best mitigate stress shielding; the local results revealed that a higher coefficient of friction led to a decrease in the magnitude of stress concentrations. Referring to Equation (1), these results were in agreement; a lower friction coefficient produced positive stress-shielding results because it caused an increase in the stress in implanted bone. As for the optimal coating location, the global results showed that the partially coated and just-pegs configurations best mitigated stress shielding; the local results supported that the fully coated and just-stem configurations correlated to a decrease in stress-concentration magnitude.

4.1. Stress-Shielding Results

The geometry of the implant greatly influences the stress-shielding behavior in bone as it affects the surface area of load transfer from implant to bone. Critical geometric features of the implant utilized in this study were the pegs and the stem. Figure 5 shows relative spikes in the stress-shielding ratios at depths of 10 mm and 40 mm, which correlated to the tip of the pegs and stem, respectively. Due to the abrupt changes in geometry at these locations, stress concentrations were produced. In combination with Equation (1), these stress concentrations created the spikes seen in the stress-shielding response of Figure 5.

A study by Completo et al. identified that bone in proximity to the stem tip or the resectioned plane experienced the highest stress shielding [21]. Another study by Au et al. analyzed the influence of pegs in the design of a tibial TKA implant with 8 mm-long pegs, and, at their apex, a notable increase in the von Mises stress was recorded in the surrounding bone [22]. The trends identified by Completo and Au at the resectioned plane and stem and peg apex aligned with the findings seen in Figure 5.

4.2. Similarity between Configurations

A consistent result across all analyses was the similar behavior between the fully coated and just-stem configurations and the partially coated and just-pegs configurations.

A source of discrepancy between these configurations was the coating of the stem. The stem was entirely coated in the fully and just-stem configurations, whereas in the partially and just-pegs configurations, the stem was only partially coated or uncoated, respectively.

It was hypothesized that the geometric dominance of the stem was a predominant factor in the stress distribution in bone. The stem was the feature of the implant with the largest footprint. Compared with the individual pegs, its surface area was 1528 mm^2 to 180 mm^2 . The stem was 38 mm in length and displaced nearly 4800 mm^3 of bone. As friction obeys $F_f = \mu N$, the specific location of the stem to experience the largest impact of friction force is where the normal forces are the largest, which is at the stem tip where the stress concentration is present. Thus, due to its geometric prominence and subsequent susceptibility to friction, the stem tip was the feature that dominated stress dispersion. Figure 9 demonstrates that the changes in stress-shielding behavior were dominated by the surface morphology applied to the implant's stem tip.

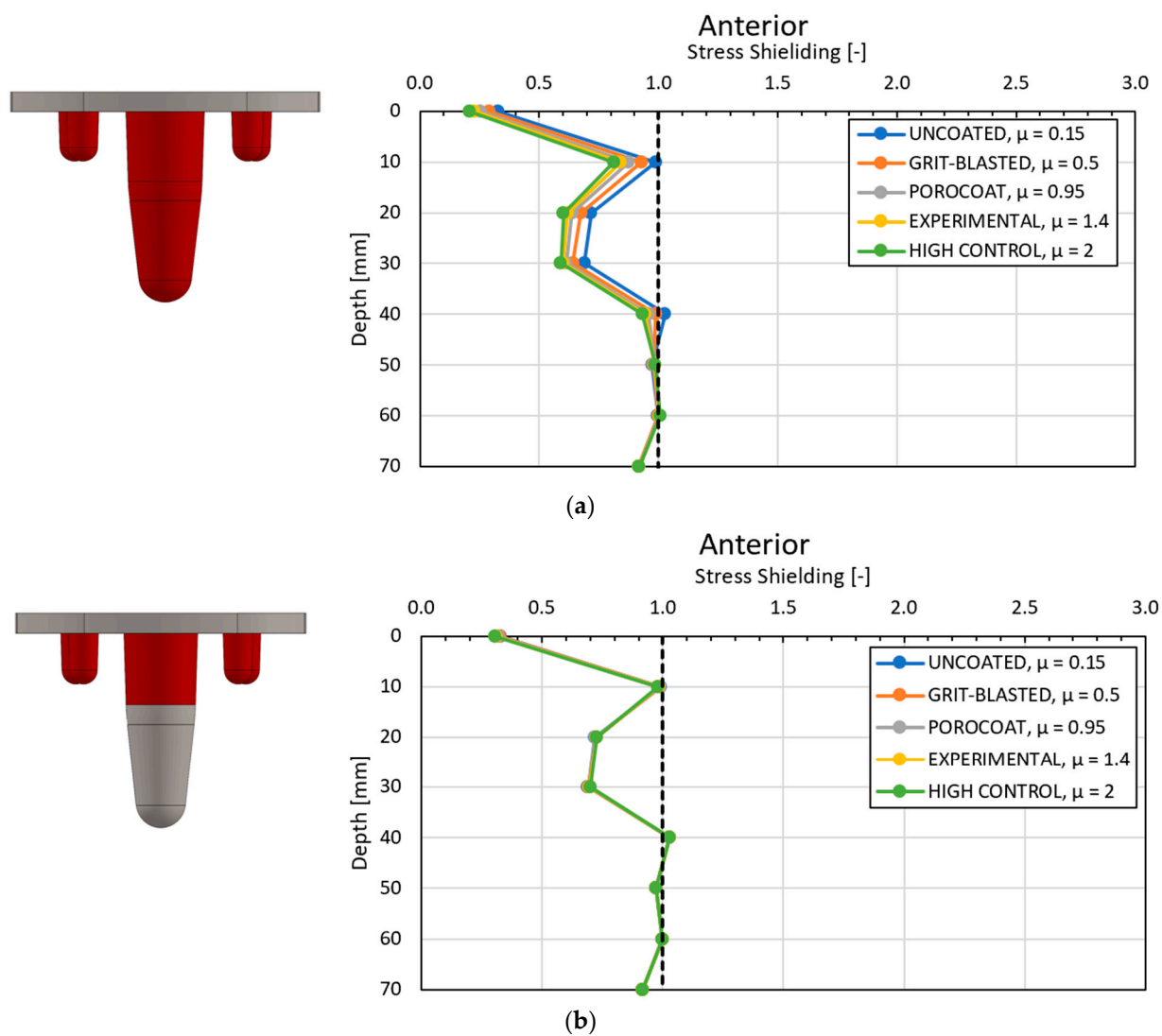


Figure 9. Cont.

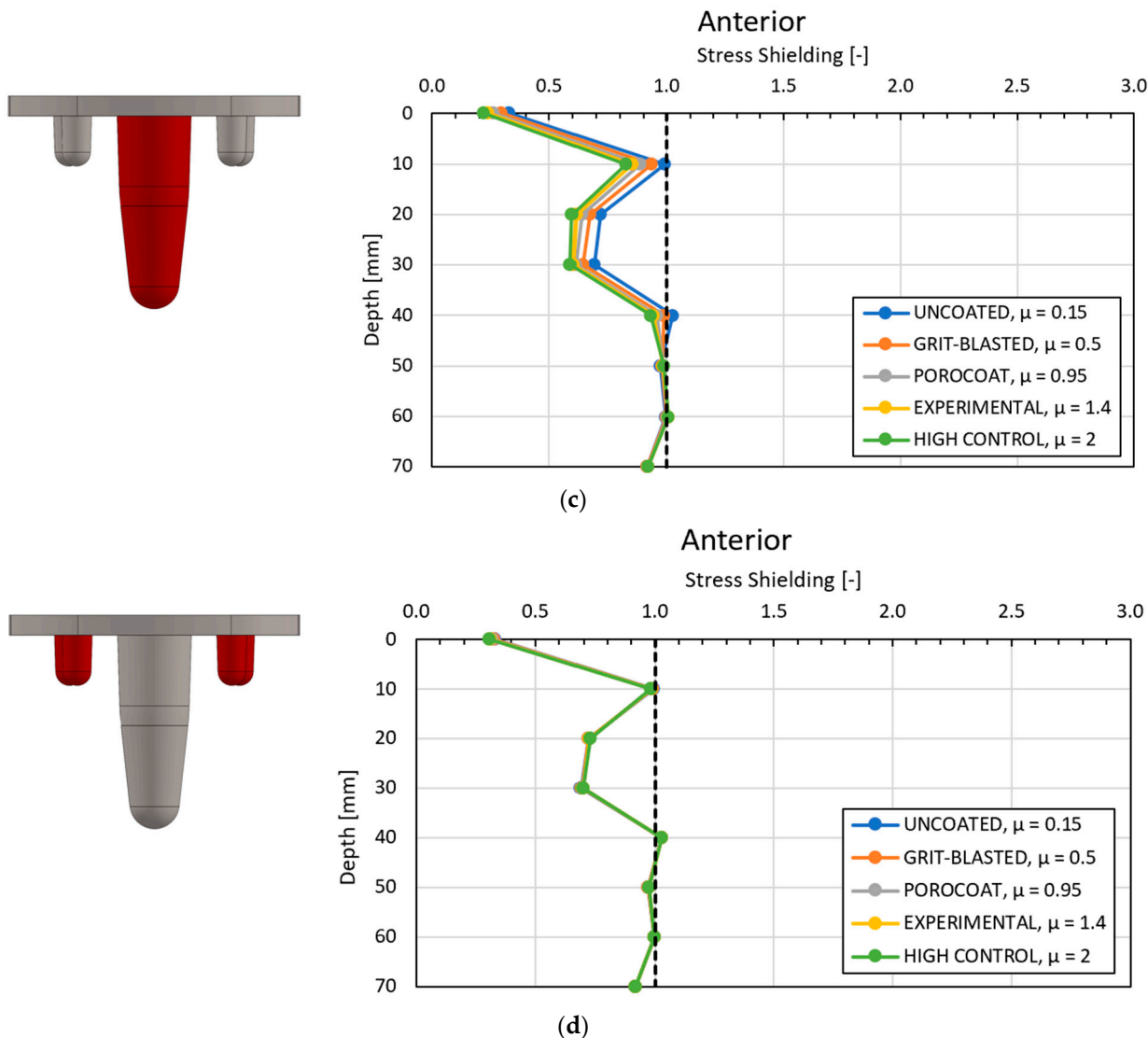


Figure 9. The coefficient of friction applied to the stem tip was the dominant factor for the stress in the tibia. The (a) fully coated and (c) just-stem configurations showed different stress-shielding responses with varying friction coefficients. The (b) partially coated and (d) just-pegs configurations did not show any appreciable difference in the stress-shielding response, demonstrating the importance of the friction coefficient applied at the stem tip. In addition, comparison of (c,d) shows that coating the pegs did not appreciably alter the stress response.

4.3. Global and Local Results

It may appear that the global and local results were contradictory. The global results concluded that a smaller coefficient of friction decreased stress shielding, while the local results showed that a smaller coefficient of friction increased localized stress concentrations. With regards to the optimal coating location, the global results found that the partially coated and just-pegs configurations best diminished stress shielding, while the local results found that the fully coated and just-stem configurations had lower magnitudes of stress concentration. However, the general conclusion is the same—a smaller coefficient of friction leads to an overall increase in stress levels in the tibia.

4.3.1. Optimal Coefficient of Friction

Stress shielding is defined as the ratio of stress experienced by implanted bone to the stress experienced by adjacent native bone. Thus, the larger the stress-shielding ratio,

the greater the stress seen in implanted bone. The global results demonstrated that stress-shielding values were inversely correlated to the friction coefficient. The local results also found stress concentrations to be inversely correlated to the friction coefficient. Thus, the global and local results support that the smaller the coefficient of friction, the greater the compressive stress experienced by bone, as seen in Figure 10.

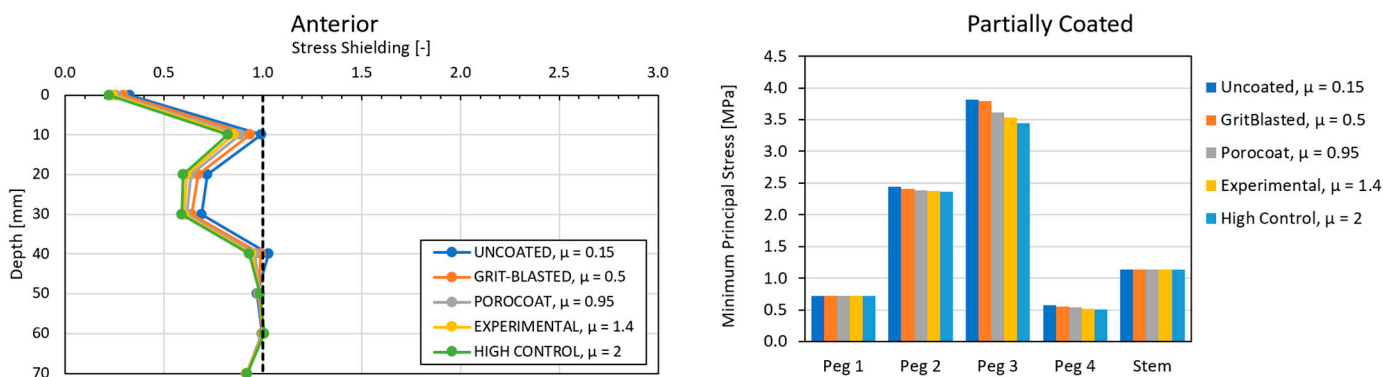


Figure 10. Comparison between global and local results for optimal coefficients of friction.

This is an interesting result, in part because of the method used to incorporate the coefficient of friction into the FEM. The frictional interface between implant and bone is governed by Coulomb's friction law, which states that $F_f = \mu N$, where F_f is the friction force, μ is the coefficient of friction, and N is the normal force. The applied force was constant across the various configurations tested; therefore, the friction force was constant across the various configurations. Therefore, in order to explain the observed trend of increased stress seen with decreasing friction coefficient, and for Coulomb's friction law to hold, as the coefficient of friction decreases, the normal force must increase.

An experimental study to determine the effects of surface morphology on the primary fixation strength of cementless femoral TKA implants by Berahmani et al. reported higher initial compressive stresses in a femoral TKA implant coated with Porocoat ($\mu = 0.95$) than implants coated with a novel coating ($\mu = 1.4$) [14]. They found lower coefficients of friction were responsible for creating higher strains on the implant surface. These findings are in agreement with the results produced by this FEM. Higher strain values would indicate a larger outward deformation of the implant, which would be responsible for the necessary increases in the normal force.

4.3.2. Optimal Coating Location

Referencing Equation (1) found the results for the optimal coating location to be in agreement—partially coated and just-pegs configurations led to greater stress levels in the tibia, as seen in Figure 11.

These results can be explained by the similarity between the configurations and the optimal coefficient of friction. The partially coated and just-pegs configurations were uncoated at the stem tip. The coefficient of friction between an uncoated titanium implant and bone is 0.15; this coefficient of friction was used to capture the uncoated bone-implant interfaces in the FEM [12]. Thus, the surface morphology at the stem tip was modeled with a friction coefficient of 0.15 for all partially coated and just-pegs configurations.

Because the stem tip of the partially and just-pegs configurations had the same surface morphologies, there were no significant differences in the stress-shielding responses. This aligns with the conclusion gathered from similarity of configurations, which showed discrepancies in the stress-shielding response to be dependent only on the surface morphology applied at the stem tip. The coefficient of friction applied to the stem tips for these configurations was 0.15; this is the smallest coefficient of friction included in the FEM, and it produced heightened stress values in the bone. This result is also in alignment with the

conclusion obtained from the analysis of the optimal coefficient of friction, which found that lower coefficients of friction caused greater levels of stress in the tibia.

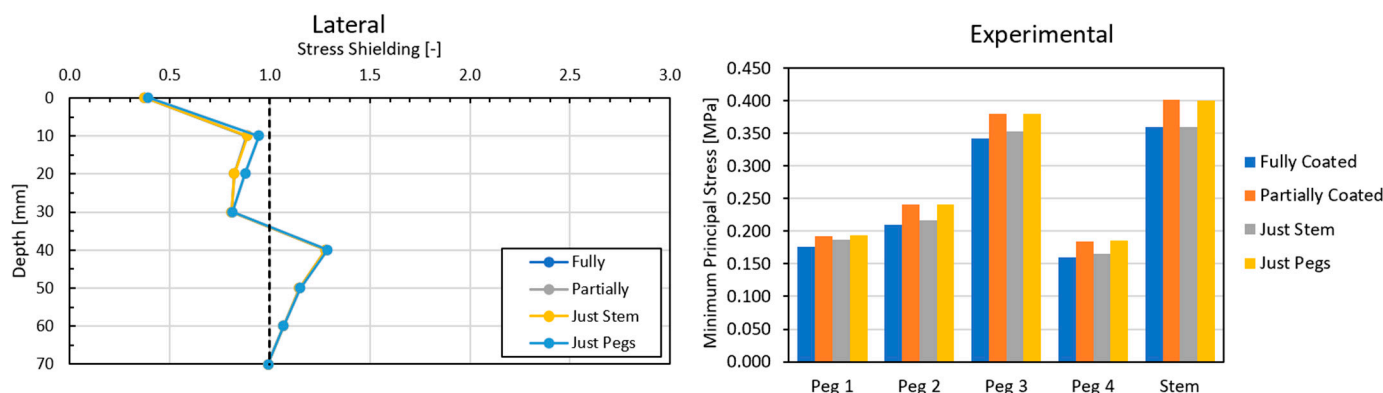


Figure 11. Comparison between global and local results for optimal coefficient of friction.

5. Conclusions

A FEM was used to compare different cementless TKA tibial implant's surface morphologies by analyzing how the stress-shielding phenomena reacted to different friction coefficients and the location of their application. It was found that stress shielding and stress concentrations are dependent on the surface morphology of the stem tip. The geometric prominence of the stem tip permits the surface morphologies applied to it to dominate the stress distribution in bone. For the surface morphologies applied to the stem tip, the results showed that decreasing coefficients of friction correlated with higher compaction of the bone, which produced increased stress levels. The larger stress levels led to more favorable stress-shielding responses but higher magnitudes of stress concentrations.

This study has important clinical implications. It has previously been experimentally established that a higher coefficient of friction leads to better stability in primary fixation [14,15]. However, our results from this study suggest that a smaller coefficient of friction mitigates the impact of the stress-shielding phenomena if applied to the stem tip. Evaluating optimal implant stability was not within the scope of this study. However from our results it can be extrapolated that an implant coated with a material that has a low coefficient of friction at the stem tip, and a material with high coefficient of friction throughout the remainder of the implant, would produce the optimal surface morphology for both primary fixation and stress shielding. Future clinical and biomechanical work should focus on evaluating the viability of this configuration, which will further elucidate how to optimize implant longevity and improve long-term patient outcomes.

Author Contributions: Conceptualization, P.J.H.; methodology, M.N., S.J.H., N.B.N. and W.A.A.; software, P.J.H. and N.B.N.; formal analysis, M.N. and W.A.A.; investigation, P.J.H.; resources, M.N., S.J.H., N.B.N. and W.A.A.; writing—original draft preparation, P.J.H.; writing—review and editing, M.N., S.J.H., N.B.N. and W.A.A.; visualization, N.B.N. and W.A.A.; supervision, M.N.; project administration, P.J.H., M.N., S.J.H., N.B.N. and W.A.A. All authors have read and agreed to the published version of the manuscript.

Funding: This research received no external funding.

Institutional Review Board Statement: Not applicable.

Informed Consent Statement: Not applicable.

Data Availability Statement: Data are contained within the article.

Conflicts of Interest: The authors declare no conflicts of interest.

References

1. Pabinger, C.; Lothaller, H.; Geissler, A. Utilization rates of knee-arthroplasty in OECD countries. *Osteoarthr. Cartil.* **2015**, *23*, 1664–1673. [[CrossRef](#)] [[PubMed](#)]
2. Memtsoudis, S.G.; della Valle, A.G.; Besculides, M.C.; Gaber, L.; Demographics, R.L.T.I.; Profiles, C. In-Hospital Complications and Mortality Associated with Primary Knee Arthroplasty. *J. Arthroplast.* **2009**, *24*, 518–527. [[CrossRef](#)]
3. Schrurs, W.B.; Hannink, G. Total joint arthroplasty in younger patients: Heading for trouble? *Lancet* **2017**, *389*, 1410–1423. [[CrossRef](#)] [[PubMed](#)]
4. Forlenza, E.M.; Serino, J., 3rd; Terhune, E.B.; Weintraub, M.T.; Nam, D.; Della Valle, C.J. Cementless Total Knee Arthroplasty is Associated With Early Aseptic Loosening in a Large National Database. *J. Arthroplast.* **2023**, *38*, S215–S220. [[CrossRef](#)] [[PubMed](#)]
5. Lum, Z.C.; Shieh, A.K.; Dorr, L.D. Why total knees fail—A modern perspective review. *World J. Orthop.* **2018**, *9*, 60–64. [[CrossRef](#)] [[PubMed](#)]
6. American Academy of Orthopaedic Surgeons (AAOS); American Joint Replacement Registry (AJRR). *2019 Annual Report*; American Academy of Orthopaedic Surgeons: Rosemont, IL, USA, 2019.
7. Kamath, A.F.; Siddiqi, A.; Malkani, A.L.; Krebs, V.E. Cementless Fixation in Primary Total Knee Arthroplasty: Historical Perspective to Contemporary Application. *J. Am. Acad. Orthop. Surg.* **2021**, *29*, e363–e379. [[CrossRef](#)] [[PubMed](#)]
8. Matassi, F.; Carulli, C.; Civinini, R.; Innocenti, M. Cemented versus cementless fixation in total knee arthroplasty. *Joints* **2014**, *1*, 121–125. [[CrossRef](#)] [[PubMed](#)]
9. Fenton, P.; Al-Nammari, S.; Blundell, C.; Davies, M. The patterns of injury and management of cuboid fractures A RETROSPECTIVE CASE SERIES. *Bone Jt. J.* **2016**, *98B*, 1003–1008. [[CrossRef](#)]
10. van der List, J.P.; Sheng, D.L.; Kleeblad, L.J.; Chawla, H.; Pearle, A.D. Outcomes of cementless unicompartmental and total knee arthroplasty: A systematic review. *Knee* **2017**, *24*, 497–507. [[CrossRef](#)]
11. Bahraminasab, M.; Sahari, B.B.; Edwards, K.L.; Farahmand, F.; Arumugam, M. Aseptic loosening of femoral components—Materials engineering and design considerations. *Mater Des.* **2013**, *44*, 155–163. [[CrossRef](#)]
12. Damm, N.B.; Morlock, M.M.; Bishop, N.E. Friction coefficient and effective interference at the implant–bone interface. *J. Biomech.* **2015**, *48*, 3517–3521. [[CrossRef](#)] [[PubMed](#)]
13. Sánchez, E.; Schilling, C.; Grupp, T.M.; Giurea, A.; Wyers, C.; van den Bergh, J.; Verdonschot, N.; Janssen, D. The effect of different interference fits on the primary fixation of a cementless femoral component during experimental testing. *J. Mech. Behav. Biomed. Mater.* **2021**, *113*, 104189. [[CrossRef](#)] [[PubMed](#)]
14. Berahmani, S.; Janssen, D.; Wolfson, D.; Rivard, K.; de Waal Malefijt, M.; Verdonschot, N. The effect of surface morphology on the primary fixation strength of uncemented femoral knee prosthesis: A cadaveric study. *J. Arthroplast.* **2015**, *30*, 300–307. [[CrossRef](#)]
15. de Vries, E.; Sánchez, E.; Janssen, D.; Matthews, D.; van der Heide, E. Predicting friction at the bone–Implant interface in cementless total knee arthroplasty. *J. Mech. Behav. Biomed. Mater.* **2022**, *128*, 105103. [[CrossRef](#)] [[PubMed](#)]
16. Berahmani, S.; Janssen, D.; Verdonschot, N. Experimental and computational analysis of micromotions of an uncemented femoral knee implant using elastic and plastic bone material models. *J. Biomech.* **2017**, *61*, 137–143. [[CrossRef](#)] [[PubMed](#)]
17. Morrison, I.B. The mechanics of the knee joint in relation to normal walking. *J. Biomech.* **1970**, *3*, 51–61. [[CrossRef](#)] [[PubMed](#)]
18. Walpole, S.C.; Prieto-Merino, D.; Edwards, P.; Cleland, J.; Stevens, G.; Roberts, I. The weight of nations: An estimation of adult human biomass. *BMC Public Health* **2012**, *12*, 439. [[CrossRef](#)] [[PubMed](#)]
19. Zhao, D.; Banks, S.A.; D'Lima, D.D.; Colwell, C.W.; Fregly, B.J. In vivo medial and lateral tibial loads during dynamic and high flexion activities. *J. Orthop. Res.* **2007**, *25*, 593–602. [[CrossRef](#)] [[PubMed](#)]
20. Fukubayashi, T.; Kurosawa, H. The contact area and pressure distribution pattern of the knee: A study of normal and osteoarthritic knee joints. *Acta Orthop.* **1980**, *51*, 871–879. [[CrossRef](#)]
21. Completo, A.; Talaia, P.; Fonseca, F.; Simões, J.A. Relationship of design features of stemmed tibial knee prosthesis with stress shielding and end-of-stem pain. *Mater Des.* **2009**, *30*, 1391–1397. [[CrossRef](#)]
22. Au, A.G.; Liggins, A.B.; Raso, V.J.; Amirfazli, A. A parametric analysis of fixation post shape in tibial knee prostheses. *Med. Eng. Phys.* **2005**, *27*, 123–134. [[CrossRef](#)] [[PubMed](#)]

Disclaimer/Publisher's Note: The statements, opinions and data contained in all publications are solely those of the individual author(s) and contributor(s) and not of MDPI and/or the editor(s). MDPI and/or the editor(s) disclaim responsibility for any injury to people or property resulting from any ideas, methods, instructions or products referred to in the content.